J. Fluid Mech. (2004), *vol.* 514, *pp.* 313–325.
DOI: 10.1017/S0022112004000515 Printed in the United Kingdom

Hypersingular boundary integrals in cusped two-dimensional free-surface Stokes flow

By MARK A. KELMANSON

Department of Applied Mathematics, University of Leeds, Leeds LS2 9JT, UK
mark@maths.leeds.ac.uk

(Received 10 February 2004 and in revised form 16 June 2004)

The biharmonic streamfunction is naturally employed in the complex-variable formulation of free-boundary transient problems in two-dimensional Stokes flow. In the event that analytical solutions are not obtainable, biharmonic boundary-integral methods (BBIMs) are frequently used. By using the well-known analytical solution of Hopper (*J. Fluid Mech.* vol. 213, 1990, pp. 349–375) for the Stokes-flow coalescence of two cylinders, it is demonstrated that the widely used direct BBIM formulation admits hypersingular integrals when solving evolving free-surface problems in the presence of a cusp, irrespective of the degree of piecewise-polynomial shape functions used to represent the curvilinear free surface. It is also shown that the hypersingularity which arises in the dynamic free-surface cusp formation is of the same fundamental form as that arising in both the static-singularity driven-cavity problem and the submergence or withdrawal of a solid plate relative to a free surface (Moffatt, *J. Fluid Mech.* vol. 18, 1964, pp. 1–18). The hypersingular BBIM integrals do not admit regularization, finite-part integration or Gauss–Chebyshev integration in the normal sense: the natural BBIM is fundamentally ill-posed in the presence of singularities born of boundary motion. In such cases, the Almansi representation should be used in order to guarantee accurate numerical solutions.

1. Introduction

Boundary-integral methods (BIMs) are well-established in the solution of static and evolving two-dimensional free-surface and interfacial flow problems in both inviscid and viscous fluid mechanics. Well-known examples of inviscid-flow BIMs include Longuet-Higgins & Cokelet (1976), Ligget (1977) and Dold & Peregrine (1986). Viscous-flow BIMs have been based on either the biharmonic streamfunction–vorticity, or direct, formulation, e.g. Kelmanson (1983*a*), Hansen (1987), Kuiken (1990, 1996), Hansen & Kelmanson (1994*b*) and Gwynllyw & Peregrine (1996), or the velocity–stress formulation, e.g. van de Vorst (1993), Pozrikidis (1997, 1998, 2001, 2003), Zinchenko, Rother & Davis (1999) and Primo, Wrobel & Power (2000). The biharmonic formulation has proved to be of fundamental importance in obtaining impressive exact solutions to certain classes of two-dimensional free-surface problems as in, e.g., Hopper (1990), Jeong & Moffatt (1992), Howison & Richardson (1995), Anatovskii (1996), Richardson (1997, 2000), Siegel (2000) and Crowdy (2003), in which the streamfunction is obtained via the Goursat representation $\psi = \mathrm{Im}(f(z) + \bar{z}g(z))$, where f and g are analytic functions of the standard complex variable z.

Exact solutions for evolving flows are, however, possible only for certain initial configurations, and the BIM is therefore applicable to a far wider class of problems.

In this paper, it is demonstrated that a critical feature of the biharmonic BIM (BBIM) of Gwynllyw & Peregrine (1996) is its use of the Almansi representation (Jaswon & Symm 1977), the real analogue of the Goursat representation, for the streamfunction. In the (direct) BBIM, coupled boundary integrals are solved for both a biharmonic ψ and a harmonic vorticity $\omega \equiv \Delta\psi$. Specifically, the biharmonic equation $\Delta\Delta\psi = 0$ is decoupled into $\Delta\psi = \omega$ and $\Delta\omega = 0$, whereafter repeated application of Green's second identity yields two coupled Fredholm integral equations of the second kind, one each for ψ and ω, in terms of both their distributions and those of their normal derivatives on the boundary. Although the precise form of the resulting boundary-integral equations varies to some degree within the direct BBIM citations, what is common to all of them is that the integrands in the Fredholm equations contain the normal vorticity gradient on the solution-domain boundary. It is demonstrated here, via a well-known analytical solution of Hopper (1990), that in the event of free-surface cusp formation, the direct BBIM admits hypersingular integrals which cannot be evaluated, even in the sense of a Cauchy principal value.

Hypersingularity has only relatively recently been addressed in the integral equations arising in the velocity–stress BIM (VSBIM) formulation, even in the absence of a cusp or boundary singularity. In evaluating the pressure inside a two-dimensional bubble, Pozrikidis (2001) obtained hypersingular integrals, finite-part integration of which was made possible only by first reducing the order of the hypersingularity by means of an interfacial condition on hydrodynamic traction. Based on the observation by Crowdy (2003) that the pressure could be obtained exactly via the Goursat representation, Pozrikidis (2003) subsequently represented the pressure as a harmonic function, circumventing the need for hypersingular integrals. In this sense, the BIM of Pozrikidis (2003) is the velocity–stress counterpart of the Almansi BBIM of Gwynllyw & Peregrine (1996).

Although we consider only two-dimensional flow, we remark that Zinchenko *et al.* (1999) report the breakdown of their three-dimensional VSBIM (which incorporates a dynamic-smoothing algorithm) in the vicinity of 'shape singularities'. Although Zinchenko *et al.* (1999) do not pursue an analysis of the 'local structure of the apparent singularities', they do report the interesting observation that, whilst true cusp-like geometries occur in two dimensions (Joseph *et al.* 1991; Joseph 1992; Jeong & Moffatt 1992), the local cusp geometry in axisymmetric three-dimensional flow is a cone. Pozrikidis (2003) further reports that, for three-dimensional flow, the evaluation of hypersingular integrals in the VSBIM requires 'strong smoothness conditions that disqualify the usage of general-purpose boundary-element methods for interfacial flow'.

It would therefore appear that, for both two- and three-dimensional flows, hypersingularity inherent in either the direct BBIM or the VSBIM has hitherto been observed, but not explicitly analysed. This motivates the present work, wherein attention is restricted to the two-dimensional biharmonic formulation, for which available exact complex-variable solutions allow us to perform an explicit analysis of the hypersingularity.

Accordingly, in § 2, the solution of Hopper (1990) is briefly reviewed and used to obtain the geometric form of the cusp in the neck between two coalescing cylinders of initially equal radius. Specifically, it is found that in scaled local Cartesian coordinates (ξ, η) centred on the (moving) cusp, the free surface at the cusp is of the parabolic form $\xi = O(\eta^{1/2})$, precisely as in the dual-roller problem of Jeong & Moffatt (1992). However, adjacent to the cusp, it is found that $\xi = O(\eta^2)$, as distinct from $\xi = O(\eta^{3/2})$ in Joseph *et al.* (1991), Joseph (1992) and Jeong & Moffatt (1992). In the present

paper, the magnitude of the parabolic cusp region is quantified and used to define a *cusp angle*. Adjacent to this parabolic region, it is demonstrated that the free surface may be approximated by low-order polynomial functions for the purposes of BBIM approximation. The 'persistence', on a macroscopic scale, of the evolving cusp is discussed in terms of its effect on the BBIM, and similarities between dynamic-cusp problems and fixed-singularity problems are identified.

In § 3, the velocity field in the neighbourhood of the cusp is used to determine the normal and tangential derivatives of the biharmonic streamfunction on the free surface near the cusp, and from these are deduced the associated free-surface vorticity and normal vorticity gradient via separation of variables (Moffatt 1964).

In § 4, the direct BBIM is outlined, and the results of § 3 are used to prove that, in the presence of a cusp or a boundary singularity, the direct BBIM formulation gives rise to coupled Fredholm integral equations in which the kernels are hypersingular, but of a form which is not amenable to regularization, finite-part integration or Gauss–Chebyshev quadrature (Korsunsky 1998): the BBIM formulation is fundamentally ill-posed. It is noted that the Almansi representation used by Gwynllyw & Peregrine (1996), primarily for reasons of efficiency, has the added bonus that it automatically remains well-posed in the presence of free-surface dynamic singularities.

2. Cusp geometry via Hopper's solution

Two infinite parallel unit-radius horizontal circular cylinders of viscous fluid are brought into tangential contact at $t=0$ along a cylindrical generator parallel with the cylinder axes. Via symmetry, the resulting Stokes flow is independent of the axial coordinate, and the two-dimensional problem is solved as the coalescence of two initially unit-radius circles centred at $(\pm 1, 0)$ in Cartesian coordinates. Gravity is assumed to be dominated by viscous and capillary forces. Hopper (1990) derives explicit forms for the parameterized coordinates of the free surface, namely

$$x(\theta, \nu) = \frac{\sqrt{2}(1-\nu^2)(1-\nu)\cos\theta}{(1-2\nu\cos 2\theta+\nu^2)\sqrt{1+\nu^2}} \tag{2.1}$$

and

$$y(\theta, \nu) = \frac{\sqrt{2}(1-\nu^2)(1+\nu)\sin\theta}{(1-2\nu\cos 2\theta+\nu^2)\sqrt{1+\nu^2}}, \tag{2.2}$$

which describe the evolving nephroid curves depicted in figure 1, in which θ is the standard plane-polar angle and ν is a quasi-time variable, obtained implicitly from the non-dimensional time t via

$$t(\nu) = \frac{\pi}{\sqrt{2}} \int_{\nu}^{1} \frac{\mathrm{d}k}{k\sqrt{1+k^2}K(k)}, \tag{2.3}$$

in which $K(k)$ is the complete elliptic integral of the first kind, given by

$$K(k) = \int_0^1 \frac{\mathrm{d}\eta}{\sqrt{(1-\eta^2)(1-k^2\eta^2)}}. \tag{2.4}$$

We are concerned only with the analysis in the neighbourhood of the cusp, present in the initial stages of evolution; this corresponds to $\nu \to 1^-$, whence $K(\nu)$ may be approximated by the asymptotic form

$$K(\nu) \sim \ln\frac{4}{\sqrt{1-\nu^2}} + O((1-\nu^2)\ln(1-\nu^2)). \tag{2.5}$$

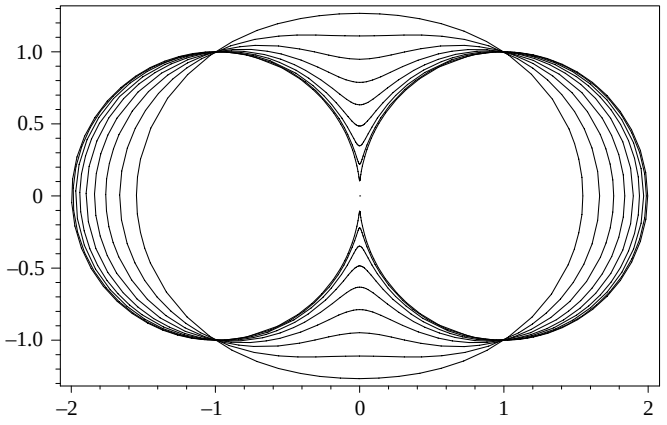

FIGURE 1. Coalescence in (x, y) space of two initally idential touching cylinders. Exact free-surface evolution given by parametric equations (2.1) and (2.2) for $\nu = 0.9(-0.1)0.1$, the first and last, via (2.3), corresponding respectively to non-dimensional times $t = 0.0638$ and $t = 2.806$.

The cusp in figure 1 occurs at $\theta = \theta_c \equiv \pi/2$. If we denote by ϵ a small perturbation in θ about θ_c then, in what follows, all leading-order asymptotic expansions will be for both $\epsilon \to 0^+$ and $\nu \to 1^-$, with a dominant error of $O(\epsilon^2, (1-\nu)^2, (1-\nu^2)\ln(1-\nu^2))$.

Referring now to figure 2, which shows the early development of the cusp in $y > 0$, we define the *cusp angle* to be the semi-angle subtended at the nadir of the cusp – referred to as the *neck* – by the symmetrically placed (about $x = 0$) points on the free surface at which the curvature changes sign. This definition is always possible in the early evolutionary phase since the free-surface curvature, given by the parametric equations (2.1) and (2.2) as

$$\kappa(\theta, \nu) = \frac{x_\theta y_{\theta\theta} - x_{\theta\theta} y_\theta}{\left(x_\theta^2 + y_\theta^2\right)^{3/2}}, \tag{2.6}$$

yields, at the neck,

$$\kappa(\theta_c, \nu) = \frac{\sqrt{1+\nu^2}(1 - 6\nu + \nu^2)}{\sqrt{2}(1-\nu)^3}, \tag{2.7}$$

which changes sign when $\nu = \nu_0 = 3 - 2\sqrt{2}$, whence (2.3) gives $t(\nu_0) \approx 2.053$; until this time, there is always a neck and therefore symmetrically disposed points where there is zero curvature. Although the general expression for $\kappa(\theta, \nu)$ is cumbersome, it is straightforward to show that the curvature vanishes when $\nu^2 + 6\nu\cos 2\theta + 1 = 0$, so that, as $\nu \to 1^-$, $\cos 2\theta \to -1/3$. Hence, to leading order, $\kappa(\theta_0, \nu) = 0$ where

$$\theta_0 \sim \theta_c \pm \tfrac{1}{2}\cos^{-1}\tfrac{1}{3}, \tag{2.8}$$

from which the cusp angle is determined as

$$\alpha(\nu) \equiv \theta_c - \tan^{-1}\frac{6\cos\frac{1}{2}\cos^{-1}\frac{1}{3} - 4}{3(1-\nu)\sin\frac{1}{2}\cos^{-1}\frac{1}{3}} = \tan^{-1}\tfrac{1}{4}(3\sqrt{2} + 2\sqrt{3})(1-\nu). \tag{2.9}$$

The series expansions, in powers of $(1-\nu)$, for both x and y in (2.1) and (2.2) leads us to analyse the (upper) cusp structure in terms of the scaled variables

$$\xi = \frac{x(\theta_c \pm \epsilon, \nu)}{(1-\nu)^2}, \qquad \eta = \frac{y(\theta_c \pm \epsilon, \nu) - y(\theta_c, \nu)}{1-\nu}, \tag{2.10}$$

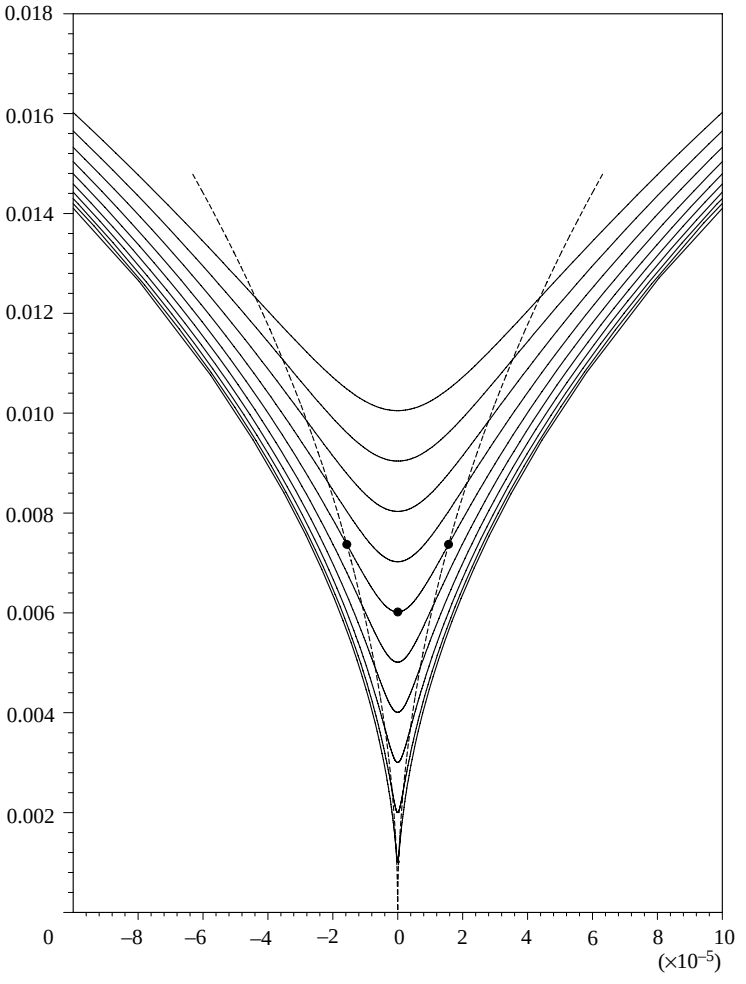

FIGURE 2. Expanded view in (x, y) space of evolving (upper) cusp region of figure 1, for $\nu = 0.999(-0.001)0.990$, the (sharp) first and (blunt) last corresponding respectively to $t = 3.17 \times 10^{-4}$ and $t = 4.17 \times 10^{-3}$. The dotted locus connect points on the evolving free surface where the curvature changes sign; these points are used to quantify the cusp angle $\alpha(\nu)$ of (2.9). For example, the angle subtended on the axis of symmetry by the three disks is $2\alpha(0.994)$. Note that the horizontal scale is approximately 100 times smaller than the vertical scale.

so that (ξ, η) are Cartesian coordinates with origin at the cusp. Expanding about $\nu = 1$, the leading-order forms of ξ and η are, from (2.1), (2.2) and (2.10),

$$\xi \sim \pm\tfrac{1}{2} \tan\epsilon \sec\epsilon, \qquad \eta \sim \sec\epsilon - 1, \tag{2.11}$$

wherein the absence of ν is noted. The physical interpretation of this is that the early stages of cusp development admit a self-similar geometry. Figure 3 reveals that (2.11) comprises an accurate approximation of (2.10) for $\nu \in [0.95, 1)$.

At leading order it is possible to eliminate ϵ from the parametric form (2.11) of the free surface to obtain an implicit formula for the scaled free-surface profile near the cusp,

$$4\xi^2 = \eta(2 + \eta)(1 + \eta)^2, \tag{2.12}$$

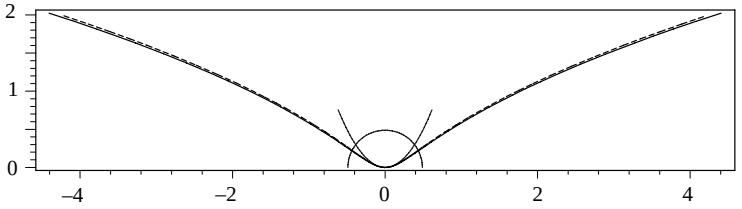

FIGURE 3. Scaled (upper) cusp profile in (ξ, η) space. The solid line is the exact solution (2.10) at $\nu = 0.95$ and the dashed line is the leading-order asymptotic behaviour (2.11). As $\nu \to 1^-$, the solid line coalesces with the dashed line, the two being optically indistinguishable on this scale for $\nu > 0.99$. The small semicircle of radius $\sqrt{\xi_0^2 + \eta_0^2}$, calculated via (2.14), intersects the free surface at those points where the curvature changes sign; inside the semicircle, the free surface is approximated by the small-ξ–small-η parabolic approximation of (2.12).

which reveals that the local neighbourhood of the cusp admits the approximation $\eta \approx 2\xi^2$, which is indicated as the small parabola on figure 3. Hence both the dynamic cusp of Hopper (1990) and the static cusp of Joseph (1992) and Jeong & Moffatt (1992) have the same (microscopic) parabolic form $\xi = O(\eta^{1/2})$ in the immediate neighbourhood of the cusp origin $(\xi, \eta) = (0, 0)$. By contrast, (2.12) reveals that the (macroscopic) cusp geometry outside the parabolic region has the asymptotic form $\xi = O(\eta^2)$ in the dynamic case, as distinct from the generic static form $\xi = O(\eta^{3/2})$ derived by Joseph (1992) and Jeong & Moffatt (1992), and corroborated experimentally in Betelú, Gratton & Diez (1998). In considering time-dependent Hele-Shaw flows driven by suction or injection in the absence of surface tension, Howison & Richardson (1995) find a dynamic $\xi = O(\eta^{3/2})$ cusp and Richardson (1999) further observes a dynamic $\xi = O(\eta^{5/2})$ cusp. The variation in these macroscopic geometries is consistent with the observation of Howison & Richardson (1995), who use the reversibility of Stokes flow to argue that an evolving cusp may assume any arbitrary form.

In order to quantify the magnitude of the parabolic region of figure 3, note that implicit differentiation of (2.12) yields the curvature of the free surface near the cusp as

$$\kappa_c = -\frac{\eta_{\xi\xi}}{\left(1 + \eta_\xi^2\right)^{3/2}} = \frac{4(\eta + 1)(2\eta^2 + 4\eta - 1)}{(4\eta^4 + 16\eta^3 + 24\eta^2 + 16\eta + 1)^{3/2}}, \tag{2.13}$$

wherein the convention has been used that the curvature is negative if the free surface is convex from within the fluid. From (2.13), the curvature changes sign when $2\eta^2 + 4\eta - 1$, whereafter (2.12) can be used to determine ξ. Hence the point on the scaled free surface where the curvature changes sign has coordinates

$$\xi_0 = \tfrac{1}{4}\sqrt{3}, \qquad \eta_0 = \sqrt{\tfrac{3}{2}} - 1. \tag{2.14}$$

The parabolic region is indicated on figure 3 as the small semicircle of radius $\sqrt{\xi_0^2 + \eta_0^2}$. Jeong & Moffatt (1992) show that the continuum formulation remains mathematically consistent at the cusp which, although having the asymptotic form $\xi = O(\eta^{3/2})$ discussed above, is in reality smoothed by finite surface tension as $\eta \to 0$. Richardson (1997) further reports that surface tension does not prevent the appearance of cusps having the asymptotic form $\xi = O(\eta^{5/2})$. When capillary smoothing does occur, the smoothing radius, for even modest capillary numbers, is on a submicron scale. Hence the parabolic region in figure 3, upon rescaling to physical (x, y) space, gives a true

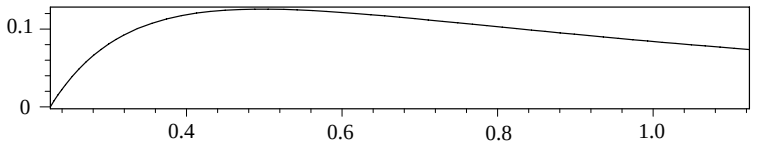

FIGURE 4. Free-surface curvature κ_c given by (2.13) in the interval $\eta \in [\eta_0, 5\eta_0]$, i.e. just outside the parabolic region of figure 3. Clearly $|\kappa_c| \ll 1$ throughout the interval so that, for the purposes of numerical approximation, the free surface there may be represented satisfactorily by low-order piecewise polynomials.

free-surface cusp on a macroscopic scale. Howison & Richardson (1995) draw attention to this 'almost-cusped' state in the presence of non-zero surface tension, in which 'curvatures are so large that the surface shape would be practically indistinguishable from a cusp even at modest values of the surface-tension parameter'. Specifically, Pozrikidis (1998) notes that the cusp curvature reveals an exponential dependence upon the capillary number, similar to that observed by Jeong & Moffatt (1992). Pozrikidis (1998) further observes that surface tension has a stabilizing effect on the cusp geometry and that there is subsequently doubt on the 'physical relevance of singular shapes at vanishing surface tension'.

Despite the representation (2.9), the cusp's exponential curvature causes it to 'persist' on a macroscopic scale beyond the initial time $\nu \equiv 1$, and this assertion is supported by figure 2, in which it is to be noted that the horizontal scale should be compressed by a factor of 100 in order to yield a physical picture. Thus, although the theoretical solution of Richardson (1997) reveals that an interface may transit through a cusp for an infinitesimal period, it is the demonstrable macroscopic near-singularity over a non-inifinitesimal period which is highly problematic to BBIMs. In this sense, dynamic cusp-like geometries have more in common with static fixed-singularity problems, such as those discussed in Moffatt (1964), than is initially apparent. In fact, it is shown in §§ 3 and 4 that there is a strong mathematical and physical link between the two. The connection between the dynamic and static problems is further highlighted in terms of implementation. Irrespective of the particular BBIM formulation used, the evolving Stokes flow is solved as a sequence of quasi-steady problems, inertial effects being introduced only via the kinematic boundary condition: the BBIM effectively models the evolution as a sequence of steady states, each of which admits a 'frozen' boundary singularity.

With the analysis of the next section in mind, it is necessary to demonstrate that the free surface adjacent to the parabolic region may be approximated by low-order polynomials. Figure 4 is a plot of κ_c given by (2.13) plotted against η in the range $[\eta_0, 5\eta_0]$. It is clear that $|\kappa_c| \ll 1$ along virtually the entirety of the curve, in figure 3, which lies adjacent to, and outside, the parabolic region. It is also clear that, upon inverse transformation to (x, y) coordinates, this section of the free surface may be adequately represented by low-order polynomials for the purposes of numerical approximation.

Finally, note that, via simple geometrical considerations, the semi-cusp angle α satisfies

$$\tan\alpha = \frac{\xi_0}{\eta_0} = \tfrac{1}{4}(3\sqrt{2} + 2\sqrt{3}) \tag{2.15}$$

which, after rescaling to (x, y) coordinates via (2.10), is in precise agreement with (2.9). Sufficient information is now available to obtain an analytical solution for the streamfunction in the neighbourhood of the cusp.

3. Streamfunction analysis near the cusp

For a general initial configuration, an exact solution will not be known and any numerical method used will necessarily approximate the evolving boundary by a piecewise-polynomial representation. For example, in Kuiken (1992, 1996), the boundary is represented by piecewise-linear elements.

The Cartesian velocity components of a moving free-surface point in the proximity of the cusp pictured in figure 1 are given by

$$u_s(\epsilon, \nu) = \frac{\mathrm{d}\nu}{\mathrm{d}t}\frac{\partial x}{\partial \nu}\bigg|_{\theta=\theta_c\pm\epsilon}, \qquad v_s(\epsilon, \nu) = \frac{\mathrm{d}\nu}{\mathrm{d}t}\frac{\partial y}{\partial \nu}\bigg|_{\theta=\theta_c\pm\epsilon}, \tag{3.1}$$

wherein $0 < \epsilon \ll 1$. Using (2.4), (2.5) and (3.1) we obtain

$$u_s(\pm\epsilon, \nu) \sim \pm\frac{\nu(1-\nu)(3+2\nu+3\nu^2)\epsilon}{\pi(1+\nu^2)(1+\nu)^2}\ln\frac{16}{1-\nu^2}, \tag{3.2}$$

$$v_s(\pm\epsilon, \nu) \sim \frac{\nu(1+\nu)}{\pi(1+\nu^2)}\ln\frac{16}{1-\nu^2}, \tag{3.3}$$

the latter revealing that v_s is, at leading order, independent of ϵ. Without loss of generality, we subsequently consider the minus signs in (3.2) and (3.3), corresponding to $\theta = \theta_c - \epsilon$, for which, on the free surface in the neighbourhood of the cusp, geometrical considerations give the operator relationship

$$\nabla_{\boldsymbol{t},\boldsymbol{n}} \equiv \mathscr{R}(\theta_c - \alpha(\nu))\,\nabla_{x,y} \tag{3.4}$$

wherein $\mathscr{R}$ is the two-dimensional rotation matrix, and $\boldsymbol{t}$ and $\boldsymbol{n}$ are a right-handed orthonormal pair on the free surface. Since the Cartesian velocity components and the standard biharmonic streamfunction ψ are related by $\boldsymbol{u} = (u, v) = (\psi_y, -\psi_x)$, (3.4) yields

$$\nabla_{\boldsymbol{t},\boldsymbol{n}}\psi \equiv \mathscr{R}(-\alpha(\nu))\boldsymbol{u}, \tag{3.5}$$

which, along with (3.2) and (3.3), provides exact (asymptotic) boundary conditions enabling the subsequent determination of the streamfunction near the cusp. On the free surface, when $\theta = \theta_c - \epsilon$, we obtain

$$\psi_t \sim -\frac{1}{4\pi}(4\epsilon + (3\sqrt{2}+2\sqrt{3}))(1-\nu)\ln\frac{16}{1-\nu^2}, \tag{3.6}$$

$$\psi_n \sim \frac{1}{2\pi}(2-(1-\nu))\ln\frac{16}{1-\nu^2}. \tag{3.7}$$

We now seek, along the lines of Moffatt (1964), a biharmonic streamfunction in the separable form $\Psi(\rho, \phi) = \rho^{\lambda+1} f_\lambda(\phi)$, where (ρ, ϕ) are two-dimensional polar coordinates centred on the cusp nadir at Cartesian coordinates $(0, y(\theta_c))$, with the $\phi = 0$ axis pointing in the negative y-direction (towards the Cartesian origin). The symmetry of the flow relative to both the $x = 0$ and $y = 0$ axes implies that Ψ is an even function of ϕ, and the conditions (3.6) and (3.7) further imply that Ψ must be of the form

$$\Psi(\rho, \phi) = \rho(A\cos\phi + B\phi\sin\phi) + O(\rho^2), \tag{3.8}$$

wherein the constants A and B are determined by applying (derived) boundary conditions (3.6) and (3.7) on $\phi = \pi - \alpha(\nu)$, i.e. on the free surface immediately to the right of the cusp. Thereafter, denoting the vorticity by $\omega \equiv \Delta_{t,n}\Psi = \Delta_{x,y}\Psi$ and the free-surface vorticity gradient by $\omega_n = \Delta_{t,n}\Psi_n$ one obtains, after expanding near $\nu = 1$,

$$\omega \sim \frac{2}{\pi^2\rho}\ln\frac{16}{1-\nu^2}, \tag{3.9}$$

$$\omega_n \sim \frac{3\sqrt{2}+2\sqrt{3}}{2\pi^2\rho^2}(1-\nu)\ln\frac{16}{1-\nu^2}, \tag{3.10}$$

both of which are independent of ϵ. Equation (3.9) reveals that, in the neighbourhood of the cusp, the vorticity (and hence the pressure or stress) field at a given point within the fluid is both inversely proportional to the distance between the point and the cusp, and independent of ϵ. This quantifies the loss of regularity of the Stokes pressure or stress field as the cusp is approached. Note that, via (3.2) and (3.3), the velocity field remains regular near the cusp.

As will be seen in the following section, formulae (3.9) and (3.10) represent a worst-case scenario for the application of a direct BBIM. Specifically, it is noteworthy that (3.9) and (3.10) yield the unexpected observation that the singularity in the Stokes flow in the vicinity of the dynamic cusp is of the identical fundamental form to that observed in the vicinity of the static corners in the driven-cavity problem of Moffatt (1964).

4. Hypersingular boundary integrals

It is to be stressed that the analytical solution for the problem of two coalescing cylinders permits us to prove the assertions in the final paragraph of § 3. Consider the integral equation

$$\psi(\boldsymbol{r}') = \int_{\partial\Omega}\left\{\frac{\partial\Delta\psi}{\partial n}G - \Delta\psi\frac{\partial G}{\partial n} + \frac{\partial\psi}{\partial n}\Delta G - \psi\frac{\partial\Delta G}{\partial n}\right\}\mathrm{d}s, \tag{4.1}$$

which expresses the value of the biharmonic function ψ at an arbitrary point $\boldsymbol{r}'$ in a region Ω, with boundary $\partial\Omega$, in terms of ψ and its derivatives on $\partial\Omega$. In (4.1), $\boldsymbol{r}' \in \Omega$, $G = G(\boldsymbol{r}, \boldsymbol{r}')$ is any fundamental solution of the biharmonic equation, all functions of ψ are evaluated at $\boldsymbol{r} \in \partial\Omega$ and $\mathrm{d}s = \mathrm{d}s(\boldsymbol{r})$. Using the notation of § 3, (4.1) becomes

$$\psi(\boldsymbol{r}') = \int_{\partial\Omega}\{\omega_n G - \omega G_n + \psi_n\Delta G - \psi\Delta G_n\}\,\mathrm{d}s, \tag{4.2}$$

in which ψ is the streamfunction. In the first stage of the BBIM, all boundary variables and the boundary geometry are approximated by piecewise polynomials, and (4.2) is collocated at selected nodes on the boundary. Although $\boldsymbol{r}' \in \partial\Omega$ at this stage, singularities arising solely through the fundamental-solution kernels are not problematic. For example, the biharmonic free-space fundamental solution has $G(\boldsymbol{r}, \boldsymbol{r}') = G(|\boldsymbol{r} - \boldsymbol{r}'|) \equiv G(r) = r^2(\ln(r) - 1)/8\pi$, from which the four kernels in the integral in (4.2) are, from left to right, $O(r^2)$, $O(r)$, $O(\ln r)$ and $O(1/r)$ as $r \to 0^+$. Hence when $\boldsymbol{r}' \in \partial\Omega$ the kernels due to G and G_n are bounded and directly integrable, whilst those due to ΔG and (the Cauchy singular) ΔG_n are evaluated as Hadamard finite-part integrals (Korsunsky 1998).

Consider now the contribution ψ_1, say, to the first term in the boundary integral in (4.2) from boundary element $\partial\Omega_C$, say, nearest to and to the right of the (upper, $y > 0$) cusp. Let the parametric integration limits for $\partial\Omega_C$ be $\rho = 0$ and $\rho = \rho_C$, say, so that

$$\psi_1(\boldsymbol{r}') \equiv \int_{\partial\Omega_C}\omega_n(\boldsymbol{r}(\rho))\,G(\boldsymbol{r}(\rho), \boldsymbol{r}')\,\mathrm{d}s(\boldsymbol{r}(\rho)) = \int_{\rho=0}^{\rho_C}\omega_n(\rho)\,G(\boldsymbol{r}(\rho), \boldsymbol{r}')\,\frac{\mathrm{d}s}{\mathrm{d}\rho}\,\mathrm{d}\rho \tag{4.3}$$

wherein $G(\boldsymbol{r}(\rho), \boldsymbol{r}') \neq 0$ when $\boldsymbol{r}' \notin \partial\Omega_C$ and $\mathrm{d}s/\mathrm{d}\rho \neq 0$ irrespective of the degree of the polynomial curve used to approximate $\partial\Omega_C$. Hence, via (3.10) and (4.3),

$$\psi_1(\boldsymbol{r}') \sim \int_{\rho=0}^{\rho_C} \frac{G(\boldsymbol{r}(\rho), \boldsymbol{r}')}{\rho^2} \frac{\mathrm{d}s}{\mathrm{d}\rho}\, \mathrm{d}\rho, \quad \rho_C \ll 1. \tag{4.4}$$

Thus $\psi_1(\boldsymbol{r}')$ is a hypersingular integral, but not in the usual sense of the kernel behaviour $G(\boldsymbol{r}(\rho), \boldsymbol{r}') = O(|\boldsymbol{r}(\rho) - \boldsymbol{r}'|^{\lambda})$ with $\lambda < -1$ and $\boldsymbol{r}' \in \partial\Omega_C$; under those circumstances, regularization, finite-part integration and Gauss–Chebyshev quadrature may be employed as in Korsunsky (1998) to approximate $\psi_1(\boldsymbol{r}')$. In this case, $\psi_1(\boldsymbol{r}')$ is strictly hypersingular due to the vorticity-gradient distribution on $\partial\Omega$ and the hypersingularity, reflected in the factor $1/\rho^2$ within the integrand in (4.4), cannot be circumvented even when $\boldsymbol{r}' \notin \partial\Omega_C$. A similar argument shows that the contribution to the second term in the boundary integral in (4.2) is also hypersingular: the direct BBIM is irretrievably ill-posed. Numerical evidence of its catastrophic failure in these circumstances is provided in Kelmanson (1983*b*) who demonstrates via the driven-cavity problem (Moffatt 1964) that the hypersingularity affects the numerical results to the extent that they are physically meaningless throughout the entire solution domain. Hence, for the dynamic cusp, as for the singularity in the driven-cavity problem, the hypersingularity is of the worst kind since contributions to the integrand from both ω and ω_n are non-integrable.

For other types of boundary singularity, e.g. Stokes flow around a re-entrant corner (Dennis & Smith 1980), one obtains (Kelmanson 1983*b*) $\omega = O(\rho^{\sigma})$ and $\omega_n = O(\rho^{\sigma-1})$, where $\sigma \in (-1, 0)$ is determined via a transcendental eigenvalue equation emanating from the boundary conditions. Then, the integral contribution from ω is integrable in the neighbourhood of the singularity, whereas that from ω_n remains hypersingular. However, the hypersingularity in this case can be removed by using the Cauchy–Riemann equations $p_s = \omega_n$ and $p_n = -\omega_s$ linking pressure p and vorticity. In the *singularity-incorporation* BBIM of Hansen & Kelmanson (1994*a*), the equation $p_s = \omega_n$ is used to integrate by parts the contribution in (4.2) involving ω_n, thereby yielding a (second) integrable contribution of $O(\rho^{\sigma})$ near the singularity. It is to be concluded that a direct BBIM of the kind implemented in Kelmanson (1983*a*), Hansen (1987) and Kuiken (1990, 1996) must always be ill-posed when considering free-surface problems in which dynamic cusps or 'worst-kind' biharmonic boundary singularities of the form $\psi \sim \rho f_0(\phi)$ (Moffatt 1964) occur.

Further to the singularity-incorporation BBIM (Hansen & Kelmanson 1994*a*), several methods have been developed to deal successfully with worst-kind biharmonic boundary singularities in fixed geometries. Kelmanson (1983*b*) proposes a *singularity-subtraction* BBIM in which a non-physical, biharmonic, quasi-streamfunction $\chi \equiv \psi - \psi_s$ is used as the boundary-integral unknown. Here, ψ_s is a truncated series of biharmonic eigenfunctions whose *a priori* unknown coefficients emerge as part of the numerical solution. One minor disadvantage of this approach is that ψ_s is singularity-dependent and needs to be recalculated (and reprogrammed) for each problem. Kelmanson & Lonsdale (1996) further propose a *singularity-annihilation* BBIM in which the natural streamfunction ψ is used, but the Green's function G is constructed to annihilate those contributions of the integrand in (4.2) containing both ω and ω_n. Although this technique is more generally applicable than both the singularity-subtraction and singularity-incorporation techniques, none is particularly suited to evolutionary flows in which the spatial coordinates of the cusp are functions of time. However, it is to be remembered that, in the numerical solution of Stokes-flow

problems, evolution enters only as a free-surface or interface update via the kinematic boundary condition, and so the static analysis is more relevant than is at first apparent.

The above discussions regarding the BBIM suggest that the BIM of Gwynllyw & Peregrine (1996) is to be strongly advocated as a superior method for solving free-surface viscous-flow problems in terms of the streamfunction. Specifically, Gwynllyw & Peregrine (1996) use the Almansi representation $\psi = y\Phi + \Theta$ (Jaswon & Symm 1977) to solve for the biharmonic streamfunction in terms of the independent harmonic functions Φ and Θ†. Gwynllyw & Peregrine (1996) adopt this approach primarily to capitalize upon the experience gained in Dold & Peregrine (1986) in the highly efficient solution of inviscid (harmonic) transient free-surface problems. However, the bonus of their Almansi formulation is that the coupled-harmonic formulation avoids the explicit use of both ω and ω_n in the boundary integrals, thereby automatically precluding the possibility of hypersingularity. As can be seen from the steepening roll waves in figures 7 to 10 of Gwynllyw & Peregrine (1996), spontaneous cusps do develop at the base of the advancing and steepening viscous wave fronts, but these do not give rise to hypersingularity in the Almansi formulation. Whilst we recall from § 2 that the analytical solution of Richardson (1997) could transit through a cusp for an infinitesimal period, the known catastrophic BBIM failure (Kelmanson 1983*b*) under 'worst-kind' conditions indicates that the direct BBIM cannot compete with the Almansi formulation for dynamic cusped flows.

In a similar vein, the alternative Almansi representation $\psi = r^2\Phi + \Theta$ used by Sadegh & Rajagopal (1980) to solve for the steady viscous flow over a static re-entrant corner is not plagued by the above-mentioned (integrable) $\omega = O(\rho^{\sigma})$ and (hypersingular) $\omega_n = O(\rho^{\sigma-1})$ in the neighbourhood of the fixed corner singularity.

Note that the Cauchy–Riemann equation $p_s = \omega_n$ reveals that the hypersingularity can be physically interpreted as a non-integrable pressure gradient along the free surface in the neighbourhood of the cusp. Precisely the same non-integrability is inherent in the submerged-plate and driven-cavity problems (Moffatt 1964) which also have $\omega = O(1/\rho)$ and $\omega_n = O(1/\rho^2)$ as $\rho \to 0^+$. Hence the present work reveals that the 'dynamic-Hopper cusp' and 'static-Moffatt singularity' both admit the identical form $p_s = O(1/\rho^2)$ for the tangential pressure gradient on the (respectively, free or fixed) domain boundary near the cusp or singularity.

Although the macroscopic continuum model evidently does not admit a mechanism to integrate this tangential pressure gradient through the cusp or singularity, progress has been achieved without the need to consider equations of motion on a microscopic scale. Hansen & Kelmanson (1994*a*) demonstrated, via their singularity-incorporation BBIM, that the seemingly unrealizable boundary conditions of the driven-cavity problem (Moffatt 1964) were indeed justified. They replaced the singularities with small 'leaks', and demonstrated convincing agreement, as the leak width was reduced to zero, between their numerical results and the analytical results of G. I. Taylor's 'scraper problem' (Taylor 1962). In doing so, they effectively relaxed the $p_s = O(1/\rho^2)$ hypersingularity condition and considered the driven-cavity problem as the singular limit of a sequence of regular, physically realistic problems. In the present case, it is clear that an analogous (surface-tension-dominated) 'hypersingularity-relaxation' mechanism must occur within the sub-micron parabolic region introduced in (2.12)

† This is to be compared with the harmonic pressure implicit in the Goursat representation underlying the modified VSBIM of Pozrikidis (2003).

and depicted in figure 3. A theoretical multi-spatial-scale resolution of this problem is beyond the scope of the present paper.

REFERENCES

Anatovskii, L. K. 1996 Formation of a pointed drop in Taylor's four-roller mill. *J. Fluid Mech.* **327**, 325–341.

Betelú, S., Gratton, R. & Diez, J. 1998 Observations of cusps during the levelling of free surfaces in viscous flows. *J. Fluid Mech.* **377**, 137–149.

Crowdy, D. G. 2003 Compressible bubbles in Stokes flows. *J. Fluid Mech.* **476**, 345–356.

Dennis, S. C. R. & Smith, F. T. 1980 Steady flow through a channel with a symmetrical constriction in the form of a step. *Proc. R. Soc. Lond.* A **372**, 393–414.

Dold, J. W. & Peregrine, D. H. 1986 An efficient boundary-integral method for steep, unsteady water waves. In *Numerical Methods for Fluid Dynamics* (ed. K. W. Morton & M. J. Baines), vol. II, pp. 671–679. Clarendon.

Gwynllyw, D. Rh. & Peregrine, D. H. 1996 Numerical simulation of Stokes flow down an inclined plane. *Proc. R. Soc. Lond.* A **452**, 543–565.

Hansen, E. B. 1987 Stokes flow down a wall into an infinite pool. *J. Fluid Mech.* **178**, 234–256.

Hansen, E. B. & Kelmanson, M. A. 1994*a* An integral equation justification of the boundary conditions of the driven-cavity problem. *Comput. Fluids* **23**(1), 225–240.

Hansen, E. B. & Kelmanson, M. A. 1994*b* Steady, viscous, free-surface flow on a rotating cylinder. *J. Fluid Mech.* **272**, 91–107.

Hopper, R. W. 1990 Plane Stokes flow driven by capillarity on a free surface. *J. Fluid Mech.* **213**, 349–375.

Howison, S. D. 1986 Cusp development in Hele-Shaw flow with a free surface. *SIAM J. Appl. Maths* **46**, 20–26.

Howison, S. D. & Richardson, S. 1995 Cusp development in free boundaries, and two-dimensional slow viscous flows. *Eur. J. Appl. Maths* **6**, 441–454.

Jaswon, M. A. & Symm, G. T. 1977 *Integral Equation Methods in Potential Theory and Elastostatics.* Academic.

Jeong, J.-T. & Moffatt, H. K. 1992 Free-surface cusps associated with flow at low Reynolds number. *J. Fluid Mech.* **241**, 1–22.

Joseph, D. D. 1992 Understanding cusped interfaces. *J. Non-Newtonian Fluid Mech.* **44**, 127–148.

Joseph, D. D., Nelson, J., Renardy, M. & Renardy, Y. 1991 Two-dimensional cusped interfaces. *J. Fluid Mech.* **223**, 383–409.

Kelmanson, M. A. 1983*a* Integral equation solution of viscous flows with free surfaces. *J. Engng Maths* **17**(4), 329–343.

Kelmanson, M. A. 1983*b* Modified integral equation solution of viscous flows near sharp corners. *Comput. Fluids* **11**(4), 307–324.

Kelmanson, M. A. & Lonsdale, B. 1996 Eddy genesis in the double-lid-driven cavity. *Q. J. Mech. Appl. Maths* **49**(4), 635–655.

Korsunsky, A. M. 1998 Gauss-Chebyshev quadratures for strongly singular integrals. *Q. Appl. Maths* **56**, 461–472.

Kuiken, H. K. 1990 Viscous sintering: the surface-tension-driven flow of a liquid form under the influence of curvature gradients at its surface. *J. Fluid Mech.* **214**, 503–515.

Kuiken, H. K. 1996 Deforming surfaces and viscous sintering. In *Mathematics of Deforming Surfaces* (ed. D. G. Dritschel & R. J. Perkins), pp. 75–97. Oxford University Press.

Liggett, J. A. 1977 Location of free surfaces in porous media. *Trans. ASCE J. Hyd. Div.* **104**, HY4, 353–365.

Longuet-Higgins, M. S. & Cokelet, E. D. 1976 The deformation of steep surface waves on water, 1: a numerical method of computation. *Proc. R. Soc. Lond.* A **350**, 1–26.

Moffatt, H. K. 1964 Viscous and resistive eddies near a sharp corner. *J. Fluid Mech.* **18**, 1–18.

Pozrikidis, C. 1997 Numerical studies of singularity formation at free surfaces and fluid interfaces in two-dimensional Stokes flow. *J. Fluid Mech.* **331**, 145–167.

Pozrikidis, C. 1998 Numerical studies of cusp formation at fluid interfaces in Stokes flow. *J. Fluid Mech.* **357**, 29–57.

Pozrikidis, C. 2001 Expansion of a compressible bubble in Stokes flow. *J. Fluid Mech.* **442**, 171–189.

Pozrikidis, C. 2003 Computation of the pressure inside bubbles and pores in Stokes flow. *J. Fluid Mech.* **474**, 319–337.

Primo, A. R. M., Wrobel, L. C. & Power, H. 2000 Low-Reynolds-number deformation of viscous drops in a bounded flow region under surface tension. *Math. Comput. Modell.* **31**, 99–118.

Richardson, S. 1997 Two-dimensional Stokes flow with time-dependent free boundaries driven by surface tension. *Eur. J. Appl. Maths* **8**, 311–329.

Richardson, S. 1999 Hele-Shaw flows with time-dependent free boundaries involving an infinite strip of fluid. *Q. Appl. Maths* **57**, 201–212.

Richardson, S. 2000 Plane Stokes flow with time-dependent free boundaries in which the fliud occupies a doubly-connected region. *Eur. J. Appl. Maths* **11**, 249–269.

Sadegh, A. M. & Rajagopal, K. R. 1980 Flow of a non-newtonian fluid past projections and depressions. *Trans. ASME: J. Appl. Mech.* **47**(3), 485–488.

Siegel, M. 2000 Cusp formation for time-evolving bubbles in two-dimensional Stokes flow. *J. Fluid Mech.* **412**, 227–257.

Taylor, G. I. 1962 On scraping viscous fluid from a plane surface. In *Miszellaneen der Angewandten Mechanik (Festschrift Walter Tollmien)* (ed. M. Schafer), pp. 313–315. Akademie-Verlag, Berlin. Reprinted in *The Scientific Papers of Sir Geoffrey Ingram Taylor*, vol. 4, pp. 410–413, Cambridge University Press, 1971.

van de Vorst, G. A. L. 1993 Integral method for a two-dimensional Stokes flow with shrinking holes applied to viscous sintering. *J. Fluid Mech.* **257**, 667–689.

Zinchenko, A. Z., Rother, M. A. & Davis, R. H. 1999 Cusping, capture, and breakup of interacting drops by a curvatureless boundary-integral algorithm. *J. Fluid Mech.* **391**, 249–292.